

A Chemical Map of NaSiCON Electrode

Materials for Sodium-ion Batteries

Baltej Singh,^{1#} Ziliang Wang,^{1#} Sunkyu Park,^{2,3,4} Gopalakrishnan Sai Gautam,⁵ Jean-Noël Chotard,^{2,4,7} Laurence Croguennec,^{3,4,6} Dany Carlier,^{3,4,6} Anthony K. Cheetham,^{1,7} Christian Masquelier,^{2,4,6,^} and Pieremanuele Canepa^{1,8 *}

¹Department of Materials Science and Engineering, National University of Singapore, Singapore
117575, Singapore

²Laboratoire de Réactivité et de Chimie des Solides (LRCS), CNRS UMR 7314, Université de Picardie Jules Verne, 80039 Amiens Cedex, France

³CNRS, Univ. Bordeaux, Bordeaux INP, ICMCB, UMR CNRS 5026, F-33600, Pessac, France

⁴RS2E, Réseau Français sur le Stockage Electrochimique de l'Energie, FR CNRS 3459, F-80039 Amiens Cedex 1, France.

⁵Department of Materials Engineering, Indian Institute of Science, Bengaluru, 560012, Karnataka, India

⁶ALISTORE-ERI European Research Institute, FR CNRS 3104, Amiens, F-80039 Cedex 1, France.

⁷Materials Department and Materials Research Laboratory, University of California, Santa Barbara, California 93106, United States

⁸Chemical and Biomolecular Engineering, National University of Singapore, 4 Engineering Drive 4, Singapore, 117585

[^]christian.masquelier@u-picardie.fr and ^{*}pcanepa@nus.edu.sg

[#]these authors contributed equally

Abstract

Na-ion batteries are promising devices for smart grids and electric vehicles due to cost effectiveness arising from the overall abundance of sodium (Na) and its even geographical distribution. Among other factors, the energy density of Na-ion batteries is limited by the positive electrode chemistry. NaSICON-based positive electrode materials are known for their wide range of electrochemical potentials,^{[1],[2],[3]} high ionic conductivity, and most importantly their structural and thermal stabilities. Using first-principles calculations, we chart the chemical space of *3d* transition metal-based NaSICON phosphates of formula $\text{Na}_x\text{MM}'(\text{PO}_4)_3$ (with M and M' = Ti, V, Cr, Mn, Fe, Co and Ni), to analyze their thermodynamic stabilities and the intercalation voltages for Na^+ ions. Specifically, we computed the Na insertion voltages and related properties of 28 distinct NaSICON compositions. We investigated the thermodynamic stability of Na-intercalation in previously unreported $\text{Na}_x\text{Mn}_2(\text{PO}_4)_3$ and $\text{Na}_x\text{VCo}(\text{PO}_4)_3$. The calculated quaternary phase diagrams of the Na-P-O-Co and Na-P-O-Ni chemical systems explain the origin of the suspected instability of Ni and Co-based NaSICON compositions. From our analysis, we are also able to rationalize anomalies in previously reported experimental data in this diverse and important chemical space.

1. Introduction

The attempt to reduce the consumption of fossil fuel resources has stimulated enormous interest in the development of the next generation of energy technologies.^{[4],[5]} Developing new battery systems capable of storing increasing quantities of energy poses extraordinary scientific and economic challenges. For several decades, lithium (Li)-ion batteries have supplied the world's portable devices, such as mobile phones, cameras, laptops, etc., but the supply chains of Li and the required transition-metals may soon be at risk due to geopolitical considerations.^{[6],[7]} In this context, sodium (Na) appears as a viable alternative to Li for battery applications due to its earth abundance, as well as the possibility of harvesting it directly from sea water. With Na being ~50 times more affordable compared to Li, Na-ion batteries (NIBs) are being explored by researchers worldwide, including a number of commercialization attempts.^[8–10] In addition, inexpensive stainless-steel current collectors are typically used in NIBs instead of the expensive copper ones found in Li-ion cells.

Positive electrode materials factor prominently in the overall energy density stored by NIBs, and the optimization of electrode chemistries to provide high intercalation voltages and gravimetric (or volumetric) capacities remains a crucial aspect in the design of competitive NIBs. In theory, transition metal layered oxide-based positive electrode materials for NIBs would offer the largest theoretical energy densities.^[10–12] However, the dominant two dimensional character of their structures affects strongly the longevity of the positive electrode material, with the electrochemical cell exhibiting a shorter-than-desired cycle life.^[12–16] Promising alternatives to layered oxides are

polyanion-based cathode materials with open and diverse anion frameworks.^[17] Polyanion positive electrode materials leverage a combination of multivalent cations (e.g., P^{5+} , Si^{4+} and S^{6+}) and anions (mostly O^{2-}) arranging into phosphate (PO_4^{3-}), silicate (SiO_4^{4-}), and sulfate (SO_4^{2-}) units, which are thermodynamically stable by virtue of the strong binding energy of their P-O, Si-O, and S-O covalent bonds.^[18–20]

Among the polyanion materials, an important class of phosphate electrodes discovered by Hong and Goodenough is the Sodium Super Ionic CONductors (NASICONs),^{[21],[22]} with the general formula $Na_xMM'(XO_4)_3$, where M and M' are metals and X = Si, P and/or S. NASICON electrode materials and electrolytes typically display significant Na^+ -mobility.^[23] The NASICON framework is important for the development of new NIB materials,^[18,23–30] since its structural tunability enables the exploration of a vast chemical space, including transition (3d, 4d) and *p*-block metals, which greatly diversifies the potential, the electrochemical properties and related structural features. In theory, an “empty” $MM'(PO_4)_3$ NASICON framework with redox-active transition metals M and M' would allow the intercalation of up to 4 Na^+ ions,^[11] which make these materials promising in terms of maximum achievable energy density.^[31] Notwithstanding the challenges of working with carbon-based anodes in NIBS,^[11,32–34] one could benefit from the presence of 4 Na^+ ions in NASICON systems such as $Na_4Mn^{II}V^{III}(PO_4)_3$.^[35,36] However, reversible extraction / intercalation of 4 Na^+ ions is still to be reported in NASICON frameworks. A reversible intercalation of 3 Na^+ ions has been recently claimed in nanostructured materials,^{[31],[37]} but more experimental and theoretical investigations are required to confirm such claims.

As an example of a NaSICON positive electrode, $\text{Na}_3\text{V}^{\text{III}}\text{V}^{\text{III}}(\text{PO}_4)_3$ (NVP) can reversibly exchange two electrons (via the activation of the $\text{V}^{\text{IV}}/\text{V}^{\text{III}}$ redox couple) delivering $\text{Na}_1\text{V}^{\text{IV}}\text{V}^{\text{IV}}(\text{PO}_4)_3$ at an average voltage of ~ 3.4 V vs. Na/Na^+ with a capacity of ~ 110 mAh/g and corresponding therefore to an energy density of ~ 370 Wh/kg.^[28,38,39] Notably, one additional Na^+ can be inserted (electro)chemically into NVP to achieve $\text{Na}_4\text{V}^{\text{II}}\text{V}^{\text{III}}(\text{PO}_4)_3$ with a voltage of ~ 1.63 V vs. Na/Na^+ . The reversible extraction of 3 Na^+ ions (i.e., starting from $\text{Na}_4\text{V}^{\text{II}}\text{V}^{\text{III}}(\text{PO}_4)_3$ as the pristine material to $\text{Na}_1\text{V}^{\text{IV}}\text{V}^{\text{IV}}(\text{PO}_4)_3$) is feasible but not practical due to the 1.8 V difference between the two processes ($\text{V}^{\text{IV}}/\text{V}^{\text{III}}$ and $\text{V}^{\text{III}}/\text{V}^{\text{II}}$) and to the difficulty in synthesizing $\text{Na}_4\text{V}_2(\text{PO}_4)_3$. In particular, Uebou et al.^[40] have demonstrated the extraction of 2.5 Na^+ ions with partial reversibility.

The versatility of NVP has been recently shown in all-solid-state NaSICON cells.^[41] Symmetric Na electrochemical cells entirely made of NaSICON frameworks adopt NVP as both electrodes; in the charged state of the battery the anode is $\text{Na}_4\text{V}^{\text{III}}\text{V}^{\text{II}}(\text{PO}_4)_3$ and the cathode $\text{Na}_1\text{V}^{\text{IV}}\text{V}^{\text{IV}}(\text{PO}_4)_3$ with $\text{Na}_3\text{Zr}_2\text{Si}_2\text{PO}_{12}$ as the electrolyte. This could deliver an average voltage of ~ 1.8 V.^[41–43] Notably, NVP suffers from poor intrinsic electronic conductivity due to the isolated VO_6 octahedra, which are never face-, edge- or corner-sharing with each other,^[26,44] in contrast to their arrangement in layered-oxide cathodes where edge-sharing exists between MO_6 moieties.^[45,46]

The Ti analogue of NVP is the Ti^{IV} -containing $\text{NaTi}^{\text{IV}}\text{Ti}^{\text{IV}}(\text{PO}_4)_3$ composition, which is stable in air and can reversibly exchange two electrons by benefitting from the $\text{Ti}^{\text{IV}}/\text{Ti}^{\text{III}}$

redox couple but at a lower voltage of ~ 2.1 V vs. Na/Na⁺ compared to that of ~ 3.4 V for V^{IV}/V^{III} redox in NVP.^[26,27] NaTi^{IV}Ti^{IV}(PO₄)₃ is also commonly used as a negative electrode material.^[29] The NaSICON Na₃Fe^{III}Fe^{III}(PO₄)₃ exhibits a voltage-composition plateau at ~ 2.5 V vs. Na/Na⁺ with a specific discharge capacity of ~ 61 mAh/g and associated to the redox couple Fe^{III}/Fe^{II}.^[47] The Fe^{IV}/Fe^{III} redox was claimed to be observed in Na₃Fe^{III}Fe^{III}(PO₄)₃ at ~ 3.4 V vs. Na/Na⁺, with a limited specific discharge capacity of ~ 22 mAh/g.^[48] Nevertheless, the formation of tetravalent iron ions has not yet been verified by any other research groups.

Importantly, Yamada *et al.*^[49] reported a voltage of ~ 4.5 V vs. Na/Na⁺ when Na⁺ is extracted from Na₃Cr^{III}Cr^{III}(PO₄)₃, which corresponds to the highest voltage ever reported among NaSICON positive electrode materials with a single type of transition metal; this is enabled by the reversible Cr^{IV}/Cr^{III} redox couple, with an initial charging capacity of ~ 98 mAh/g. Importantly, the Mn, Co and Ni, Na_xM₂(PO₄)₃ NaSICON analogues have not yet been reported.

The high voltage delivered by the Cr^{IV}/Cr^{III} redox couple offers scope for exploring new high-voltage and high-capacity materials using more than one transition metal, e.g., Na₄Cr^{III}Mn^{II}(PO₄)₃.^{[31],[37]} Other NaSICON materials, such as Na₃V^{III}Cr^{III}(PO₄)₃,^[50] Na₂Ti^{IV}V^{III}(PO₄)₃,^{[51],[52]} Na₃Ti^{IV}Mn^{II}(PO₄)₃,^{[53],[54]} Na₂Ti^{IV}Fe^{III}(PO₄)₃,^[55] Na₄V^{III}Mn^{II}(PO₄)₃,^{[35],[36],[56],[57]} Na₃V^{III}Fe^{III}(PO₄)₃^[30,36] and Na₄V^{III}Ni^{II}(PO₄)₃,^[36] have also been studied to enable high reversible capacity, longevity and as anode and cathode electrodes.

In order to access three electrons (i.e., 3 Na⁺ ions per 2 transition metals per formula unit) in any mixed transition-metal NaSICON, two criteria must be met: i) the transition metal must be in the +2 and +3 oxidation states in the fully discharged state (i.e., 4 Na⁺ ions), and ii) at least one of the transition metals must accommodate multiple redox active oxidation states. Compounds that meet these criteria are mainly either Mn or V containing ones, for example Na₂Ti^{IV}V^{III}(PO₄)₃, Na₃Ti^{IV}Mn^{II}(PO₄)₃, Na₄Mn^{IV}V^{III}(PO₄)₃, and Na₄Cr^{III}Mn^{II}(PO₄)₃, which undergo reversible electrochemical reactions involving up to three electrons with average voltages of ~2.4, ~3.2, ~3.4, and ~4.1 V vs. Na/Na⁺, respectively. While Na₄Cr^{III}Mn^{II}(PO₄)₃ exhibits a particularly high theoretical energy density of ~566 Wh kg⁻¹ for a gravimetric capacity of ~160 mAh g⁻¹,^[31] only ~40 mAh g⁻¹ was reported at voltages below 1.6 V vs. Na/Na⁺. However, there remains a wide chemical space yet to be explored, which could yield new combinations of transition metals enabling improved NaSICON positive electrode materials. A systematic study, either experimental or theoretical, of trends in voltages and phase behavior of possible transition-metal combinations within NaSICON positive electrode materials has not yet been reported.

Here, we present a first-principles study that charts the chemical space of 28 different Na_xMM'(PO₄)₃-electrode chemistries, where M and M' can be any of the 3d transition metals, Ti, V, Cr, Mn, Fe, Co and Ni, with Na content varying in the range 1 ≤ x ≤ 4. We derive the intercalation voltages for all the 28 Na_xMM'(PO₄)₃ systems, validate our predictions with available experimental data, and identify promising NaSICON compositions to be targeted experimentally. Specifically, we find new promising or not fully explored Na_xMM'(PO₄)₃ compositions, such as Na_xMn₂(PO₄)₃

($1 \leq x \leq 4$), $\text{Na}_x\text{Co}_2(\text{PO}_4)_3$ ($3 \leq x \leq 4$), $\text{Na}_x\text{TiCo}(\text{PO}_4)_3$ ($2 \leq x \leq 4$), $\text{Na}_x\text{VCo}(\text{PO}_4)_3$ ($1 \leq x \leq 4$), $\text{Na}_x\text{CrCo}(\text{PO}_4)_3$ ($2 \leq x \leq 4$), $\text{Na}_x\text{CoMn}(\text{PO}_4)_3$ ($2 \leq x \leq 4$) and $\text{Na}_x\text{CrFe}(\text{PO}_4)_3$ ($2 \leq x \leq 4$). We do not comment on the insertion mechanism of Na^+ ions, i.e. the competition between solid solution vs. phase separation, but focus on the propensity for Na^+ ion to intercalate in each NaSICON host. Also, we analyze the possible origins of the difficulties in synthesizing specific NaSICON chemistries. Finally, by analyzing the computed quaternary phase diagrams we reveal why $\text{Na}_x\text{M}_2(\text{PO}_4)_3$ (M= Mn, Co and Ni) NaSICON compounds have never been reported experimentally.

2. Results:

2.1 Structural features of $\text{Na}_x\text{MM}'(\text{PO}_4)_3$ electrodes

Depending on the transition-metal, temperature and/or Na content (x) per formula unit (f.u.) NaSICON materials adopt typically a rhombohedral ($R\bar{3}c$),^[49,58] an ordered monoclinic ($C2/c$ or Cc),^[21,22,50] or, in the specific case of $\alpha\text{-Na}_3\text{Ti}^{\text{III}}\text{Ti}^{\text{III}}(\text{PO}_4)_3$, a triclinic structure ($P1$).^[59] For example, $\text{Na}_4\text{V}^{\text{II}}\text{V}^{\text{III}}(\text{PO}_4)_3$ and $\text{Na}_4\text{Fe}^{\text{II}}\text{Fe}^{\text{III}}(\text{PO}_4)_3$ ^[60] are rhombohedral, while $\text{Na}_3\text{V}^{\text{III}}\text{V}^{\text{III}}(\text{PO}_4)_3$,^[58] $\text{Na}_3\text{Fe}^{\text{III}}\text{Fe}^{\text{III}}(\text{PO}_4)_3$,^[47] $\text{Na}_3\text{Ti}^{\text{III}}\text{Ti}^{\text{III}}(\text{PO}_4)_3$ and $\text{Na}_3\text{Cr}^{\text{III}}\text{Cr}^{\text{III}}(\text{PO}_4)_3$ form monoclinic^[59] structures at room temperature due to Na/vacancy orderings. **Figure 1** shows the archetypal structure of the rhombohedral $\text{Na}_x\text{MM}'(\text{PO}_4)_3$.

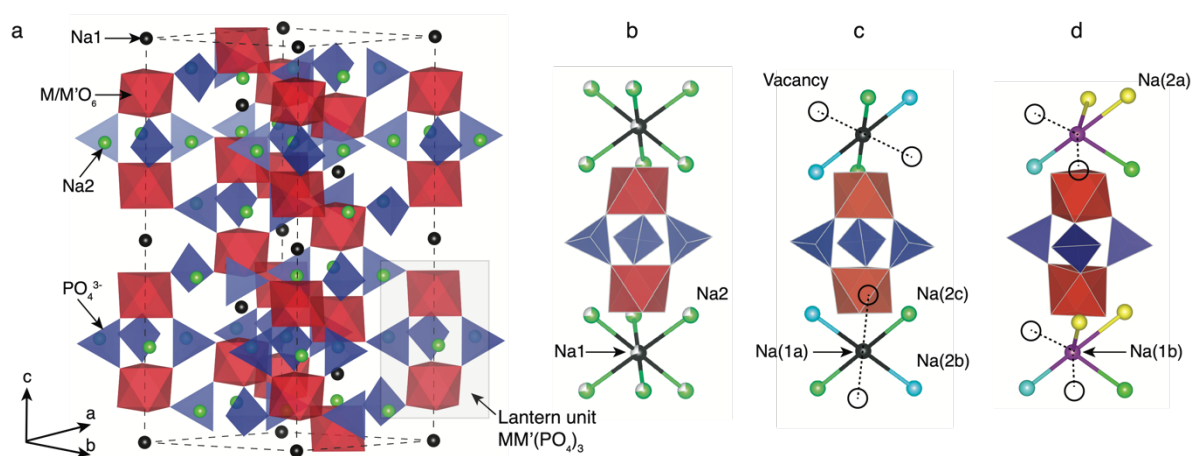


Figure 1 **a** The rhombohedral ($R\bar{3}c$) structure of $\text{Na}_4\text{MM}'(\text{PO}_4)_3$ with M and $M' = \text{Ti, V, Cr, Mn, Fe, Co}$ and Ni . The “lantern unit” is made up of two MO_6 (or $\text{M}'\text{O}_6$) octahedra (red) sharing corners with PO_4^{3-} tetrahedra (blue). The gray box in (a) highlights the arrangement of lantern units. Two distinct Na ions, i.e. Na1 (black) and Na2 (green), are present in the rhombohedral NaSICONs. Panel **b** lantern representation of the Na disordering (with partial Na occupancies on Na1 and Na2 sites) in the rhombohedral $\text{Na}_3\text{MM}'(\text{PO}_4)_3$ polymorph. Panel **c** shows one of the lantern representations of the complete ordering of Na^+ ions in the corresponding $\text{Na}_3\text{MM}'(\text{PO}_4)_3$ monoclinic ($C2/c$) phase, whereas panel **d** shows the local environment of sites Na1b (violet) and Na2a (yellow) in the same monoclinic arrangement. Vacancies are represented by open circles.

$\text{Na}_x\text{MM}'(\text{PO}_4)_3$ materials consist of $(M, M')\text{O}_6$ octahedral and PO_4 tetrahedral units. As

shown in **Figure 1**, 3 PO₄ tetrahedra share all their corners with two (M,M')O₆ octahedra forming the so called “lantern units” —a recurrent motif of NaSICON structures. The lantern units assemble into a 3-D MM'(PO₄)₃ framework producing two types of available sites for Na in the rhombohedral phase (**Figure 1b**): Na1 (one per f.u.) and Na2 (three per f.u.). The six-coordinated Na1 sites are located between two (M,M')O₆ octahedra, while the Na2 sites remain eight-coordinated by the O atoms of the PO₄ tetrahedra. At x = 4 in Na_xMM'(PO₄)₃, all the Na positions (i.e. 1 x Na1 and 3 x Na2 per f.u.) are fully occupied and the structure is ordered and rhombohedral. In several NaSICONs, the Na⁺ ions are fully ordered at x = 3 and the structure adopts monoclinic (*C2/c*) symmetry (**Figure 1c**), where the Na1 site splits into two distinct sites (i.e., fully occupied Na1a and Na1b). The Na2 site splits into five sites (3 fully occupied, Na2a, Na2b and Na2c, and 2 vacancies).

2.2 Na intercalation in Na_xM₂(PO₄)₃ NaSICONs

The energetics of Na intercalation and the corresponding average voltages (see methodology in **Section 5**) for single transition metal (M=M') NaSICON electrodes are shown in panels **a** and **b** of **Figure 2**. The computed formation energies for the most stable orderings in Na_xM₂(PO₄)₃ are displayed in **Figure 2a** as a function of Na concentration, where the lower energy envelopes form the so-called convex hull (solid lines) for a given Na_xM₂(PO₄)₃ system. The convex hull highlights the thermodynamic phase behavior at 0 K of Na (de)intercalation from/into the Na_xM₂(PO₄)₃ frameworks. Since the convex hull at 0 K does not include any entropic and *pV* effects, it informs

on the propensity of Na to bond with the $M_2(PO_4)_3$ frameworks. Among the $M = Ti, V, Cr, Mn, Fe, Co$ and Ni compounds, NaSICONs based on Ti, V, Cr and Fe have been reported experimentally.^{[29],[38],[49],[47],[48]} From previous experimental work, the redox activities of Ti and V provide accessible Na concentrations ranging in $1 \leq x \leq 4$, while $Na_xCr_2(PO_4)_3$ spans a narrower range of Na concentration ($1 \leq x \leq 3$), being limited by the Cr^{IV}/Cr^{III} redox couple. Notably, the Cr^{III}/Cr^{II} redox couple has not been cycled reversibly in NaSICON frameworks so far.

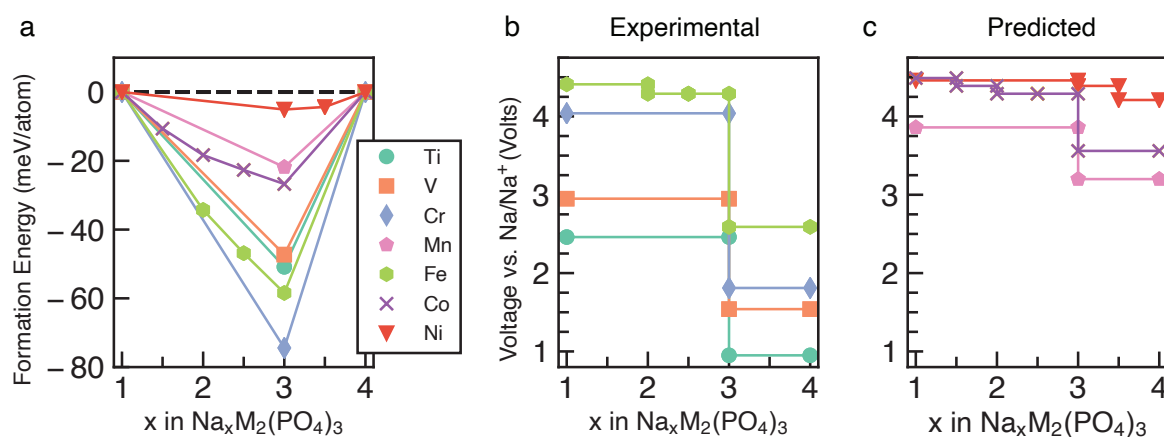


Figure 2 Panel **a** shows the computed formation energies and respective convex hulls for Na vacancy orderings as a function of Na concentration (x) in $Na_xM_2(PO_4)_3$ where $M = Ti, V, Cr, Mn, Fe, Co$ and Ni . Panels **b** and **c** show the intercalation voltages vs. Na/Na^+ for the experimentally known ($M = Ti, V, Cr$ and Fe) and predicted ($M = Mn, Co$ and Ni) $Na_xM_2(PO_4)_3$ compounds, respectively. Only the stable orderings forming the convex hull are displayed in panel **a**. The energies of unstable configurations for each convex hull are shown in **Figures S1-S7** of the SI.

The structures represented by specific Na/vacancy orderings falling above the convex hull are thermodynamically unstable/metastable and are shown in **Figures S1-S7** of the **Supporting Information (SI)**. Note that the unstable Na/vacancy orderings should decompose to the closest ground state(s) identified by the convex hulls of **Figure 2a**. For example, in **Figure S2**, $Na_2V_2(PO_4)_3$ (*C2*) is found to be slightly metastable (~ 1.8 meV/atom above the stability line) and will phase separate into $Na_1V^{IV}V^{IV}(PO_4)_3$ and $Na_3V^{III}V^{III}(PO_4)_3$. Consequently, the stable structures lying on the convex hull (e.g.,

$\text{Na}_3\text{V}^{\text{III}}\text{V}^{\text{III}}(\text{PO}_4)_3$) give rise to a “step” in the calculated Na voltage curve (see **Figure S2**). The convexity, that is the depth of the convex hull, is an indication of the thermodynamic stabilities of the specific Na/vacancy configurations. The calculated ground states on the convex hull do not necessarily correspond to topotactic structures since we allow changes to the symmetry (e.g., rhombohedral \rightarrow monoclinic) of the host during deintercalation of Na from $\text{Na}_4\text{MM}'(\text{PO}_4)_3$ in our calculations.

Analyzing **Figures 2a** and **2b**, the following general trends can be deduced:

- i) The end member compositions in $\text{Na}_x\text{M}_2(\text{PO}_4)_3$, i.e. $x = 1$ and 4 , typically adopt the rhombohedral ($R\bar{3}c$ or $R\bar{3}$) space group. Exceptions to this trend are $\text{Na}_4\text{Cr}^{\text{II}}\text{Cr}^{\text{III}}(\text{PO}_4)_3$ and $\text{Na}_4\text{Mn}^{\text{II}}\text{Mn}^{\text{III}}(\text{PO}_4)_3$, which are predicted to have triclinic ($P\bar{1}$) symmetry due to Jahn-Teller distortions of high-spin Cr^{2+} and Mn^{3+} d^4 ions. These have not yet been-observed experimentally.
- ii) A global minimum in the formation energy curves, i.e., the highest magnitude of formation energy, is present across all transition-metal $\text{Na}_x\text{M}_2(\text{PO}_4)_3$ systems at $x = 3$ (**Figure 2a**).^[43]
- iii) Among all the $\text{Na}_3\text{M}^{\text{III}}\text{M}^{\text{III}}(\text{PO}_4)_3$ compounds investigated, $\text{Na}_3\text{Cr}^{\text{III}}\text{Cr}^{\text{III}}(\text{PO}_4)_3$ displays the deepest or lowest (i.e. most favorable) formation energy, followed by $\text{Na}_3\text{Fe}^{\text{III}}\text{Fe}^{\text{III}}(\text{PO}_4)_3 > \text{Na}_3\text{Ti}^{\text{III}}\text{Ti}^{\text{III}}(\text{PO}_4)_3 \approx \text{Na}_3\text{V}^{\text{III}}\text{V}^{\text{III}}(\text{PO}_4)_3$ respectively, which reflects the stability of the M^{3+} oxidation states of these transition metals. The stability of $\text{Na}_3\text{Cr}^{\text{III}}\text{Cr}^{\text{III}}(\text{PO}_4)_3$, in particular, is enhanced by the large ligand field stabilization energy of the Cr^{3+} ($3d^3$) cation. The other compounds, $\text{Na}_3\text{Co}^{\text{III}}\text{Co}^{\text{III}}(\text{PO}_4)_3$, $\text{Na}_3\text{Mn}^{\text{III}}\text{Mn}^{\text{III}}(\text{PO}_4)_3$ and $\text{Na}_3\text{Ni}^{\text{III}}\text{Ni}^{\text{III}}(\text{PO}_4)_3$, display shallower

(i.e. less favorable) formation energies (< 25 meV/atom, **Figure 2a**). The shallow convex hulls for $\text{Na}_x\text{Mn}_2(\text{PO}_4)_3$ and $\text{Na}_x\text{Ni}_2(\text{PO}_4)_3$ are caused by the Mn^{3+} and Ni^{3+} ions which are both Jahn-Teller active. The computed magnetic moment of Co^{3+} $\text{Na}_3\text{Co}^{\text{III}}\text{Co}^{\text{III}}(\text{PO}_4)_3$ is $\sim 3.0 \mu_B$, indicating an intermediate spin state and possible Jahn-Teller activity.

- iv) Unsurprisingly, the deep minima in the convex hull plot of **Figure 2a** lead to a large voltage step as shown in **Figures 2b** and **2d**, following the sequence $\text{Cr} > \text{Fe} > \text{Ti} > \text{V} > \text{Co} > \text{Mn} > \text{Ni}$.
- v) The M(III/II) redox couples that correspond to Na contents from $x = 3$ to $x = 4$, follow the voltage trend $\text{Ni} > \text{Co} > \text{Mn} > \text{Fe} > \text{Cr} > \text{V} > \text{Ti}$, while the M(IV/III) couples ($x = 1$ to $x = 3$) follow the sequence $\text{Ni} > \text{Co} > \text{Fe} > \text{Cr} > \text{Mn} > \text{V} > \text{Ti}$. Thus, Ni and Co (V and Ti) display the highest (lowest) average voltages for both M redox couples.

To validate our methodology, we have benchmarked our results against experimental observations in $\text{Na}_x\text{V}_2(\text{PO}_4)_3$, which has been extensively studied.^{[58],[61]} Experimentally, $\text{Na}_3\text{V}^{\text{III}}\text{V}^{\text{III}}(\text{PO}_4)_3$ adopts monoclinic symmetry ($C2/c$) at room temperature, which is in qualitative agreement with our DFT calculations identifying the monoclinic ordering (Cc) as the stable structure at $x = 3$. From **Figure 2a**, $\text{Na}_3\text{V}^{\text{III}}\text{V}^{\text{III}}(\text{PO}_4)_3$ is on the convex hull with $\text{Na}_1\text{V}^{\text{IV}}\text{V}^{\text{IV}}(\text{PO}_4)$ and $\text{Na}_4\text{V}^{\text{II}}\text{V}^{\text{III}}(\text{PO}_4)_3$, which adopt the rhombohedral space groups $R\bar{3}c$ and $R\bar{3}$, respectively, in our calculations; this is consistent with X-ray diffraction experiments.^{[62],[38],[58]} In **Figure 2b**, the extraction of 2 Na atoms from $\text{Na}_3\text{V}^{\text{III}}\text{V}^{\text{III}}(\text{PO}_4)_3$ gives rise to an average voltage of ~ 2.96 V vs. Na/Na^+ and corresponds to the $\text{V}^{\text{IV}}/\text{V}^{\text{III}}$ redox, while the insertion of Na into

$\text{Na}_3\text{V}^{\text{III}}\text{V}^{\text{III}}(\text{PO}_4)_3$ results in a voltage of 1.54 V (associated with the $\text{V}^{\text{III}}/\text{V}^{\text{II}}$ redox). Experimentally, both the V redox couples ($\text{V}^{\text{IV}}/\text{V}^{\text{III}}$ and $\text{V}^{\text{III}}/\text{V}^{\text{II}}$) are involved in two-phase reaction mechanisms, yielding average voltages of ~ 3.40 V and ~ 1.63 V vs. Na/Na^+ , respectively,^[61] which are in reasonable agreement with our computed values. Notably, both GGA+ U and hybrid functionals underestimate the computed voltages of $\text{Na}_x\text{V}_2(\text{PO}_4)_3$ (see **Section S2** in SI). Another important assessment to verify the validity of our simulations is ensuring that changes in oxidation states of the transition metals upon Na extraction/insertion are captured. We verify that the correct redox processes do occur in our calculations by tracking the on-site magnetic moments on the transition metal atoms (**Table S1**), as well as the transition metal coordination environments (**Table S2**), which are discussed in **Section S3** of the SI.

Whenever we could not assign the expected oxidation state of the transition metals directly from the computed magnetic moments (e.g., in cases of Fe, Co and Ni based NaSICONs), we inspected the appropriate density of states (DOS). The DOS are reported in **Section S4** of the SI (**Figures S9-S12**). As an example, we show in **Figure 3**, the total and atom-projected DOS in $\text{Na}_x\text{V}_2(\text{PO}_4)_3$, for $x = 1, 3$ and 4 , which are the ground states identified in **Figure 2**. The DOS are displayed for spin up and spin down states in the range of interest (-2.5 — 2 eV) around the Fermi energy. Unless a given structure is metallic, the top of the Fermi energy is arbitrarily set to the top of the valance band.

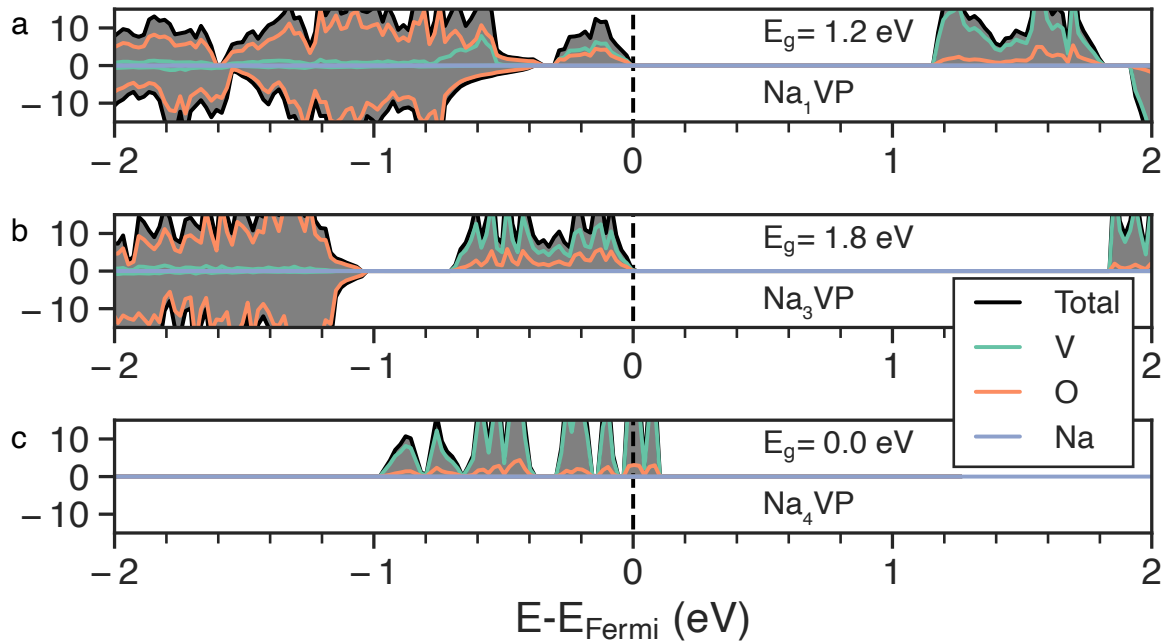


Figure 3 The total (gray) and atom projected (V aqua, O orange and Na blue) DOS of $\text{Na}_x\text{V}_2(\text{PO}_4)_3$ NaSICON (NVP), where for Na concentrations $x = 1, 3$ and 4 . The vertical line denotes the Fermi energy level and E_g is the calculated band gap at the GGA+ U level of theory.

Panels **a** and **b** in **Figure 3** show the results for $\text{Na}_1\text{V}^{\text{IV}}\text{V}^{\text{IV}}(\text{PO}_4)_3$ and $\text{Na}_3\text{V}^{\text{III}}\text{V}^{\text{III}}(\text{PO}_4)_3$, respectively. From the projected DOS, the valence bands near the Fermi energy are occupied by 3d electrons of vanadium (aqua line), while the 2p O states (orange line) lie at lower energies. In general, the vanadium 3d states tend to dominate the valence band and shift at higher energies as more Na is inserted, closing the band gap ($> 1\text{ eV}$ for both compounds). However, the monoclinic distortion of $\text{Na}_3\text{V}^{\text{III}}\text{V}^{\text{III}}(\text{PO}_4)_3$ is responsible for an increase in band gap ($\sim 1.8\text{ eV}$) contrary to the $\text{Na} = 1$ and $\text{Na} = 4$ trends. As expected, the intercalation of more Na^+ ions as in $\text{Na}_4\text{V}^{\text{III}}\text{V}^{\text{II}}(\text{PO}_4)_3$ (**Figure 3 c**) increases (destabilizes) further the valence band, with this composition becoming gapless and a Fermi energy dominated by V(3d) states when GGA+ U is used. For the $\text{Na}_4\text{V}^{\text{III}}\text{V}^{\text{II}}(\text{PO}_4)_3$, the band gap opens to $\sim 0.3\text{ eV}$ when the more accurate HSE06 hybrid functional is used at the relaxed HSE06 structure. Very recent hybrid functional

simulations on $\text{Na}_x\text{Ti}_2(\text{PO}_4)_3$ have verified these orders of magnitudes, with $\text{Na}_4\text{Ti}^{\text{III}}\text{Ti}^{\text{II}}(\text{PO}_4)_3$ showing a small band gap of ~ 0.59 eV.^[63]

In the case of $\text{Na}_x\text{Ni}_2(\text{PO}_4)_3$ the projected DOS of **Figure S12** suggests metallic behavior at all the Na concentrations explored (i.e., $x = 1, 3$ and 4). $\text{Na}_x\text{Mn}_2(\text{PO}_4)_3$ and $\text{Na}_x\text{Co}_2(\text{PO}_4)_3$ show band gaps >1.0 eV at $x = 3$ and 4 , but become metallic at $x = 1$, as shown by **Figures S9** and **S11**. $\text{Na}_1\text{Fe}^{\text{IV}}\text{Fe}^{\text{IV}}(\text{PO}_4)_3$ also appears, surprisingly, metallic (**Figure S10**), which introduces difficulties in localizing the $\text{Fe}^{\text{III}}/\text{Fe}^{\text{IV}}$ redox couple. Therefore, due to the apparent metallic behavior of some of these systems (Fe, Co and Ni-based NaSICONs), we were unable to assign unique oxidation states to their transition metals. Notably, DFT is a ground state theory and not adequate in the prediction of accurate band gaps.^[64]

2.3 Na^+ ion intercalation in $\text{Na}_x\text{MM}'(\text{PO}_4)_3$ NaSICON structures

We extend our analysis to the reversible extraction of Na from mixed $\text{Na}_4\text{MM}'(\text{PO}_4)_3$ compounds where, for the sake of simplicity, the ratio $\text{M}:\text{M}'$ is fixed as 1:1. While all the $\text{M}:\text{M}'$ combinations have been considered, to simplify our discussion we concentrate on the cases where $\text{M} = \text{Ti}$, while $\text{M}' = \text{Ti}, \text{V}, \text{Cr}, \text{Mn}, \text{Fe}, \text{Co}$ and Ni . Other mixed $\text{Na}_4\text{MM}'(\text{PO}_4)_3$ are reported in **Section S5** of the SI (**Figures S13-S33**). The main reason behind choosing Ti-based mixed TM NaSICONs is their maximum experimental electrochemical data availability as compared to other combinations. **Figures 4a** and **4b** show the calculated convex hulls for experimentally reported and

theoretical $\text{Na}_x\text{TiM}'(\text{PO}_4)_3$ compounds, respectively, with Na contents in the range $1 \leq x \leq 4$. **Figure 4c** displays the corresponding voltages. $\text{Na}_x\text{Ti}_2(\text{PO}_4)_3$ is also reported in **Figures 4a** and **4c** as a reference.

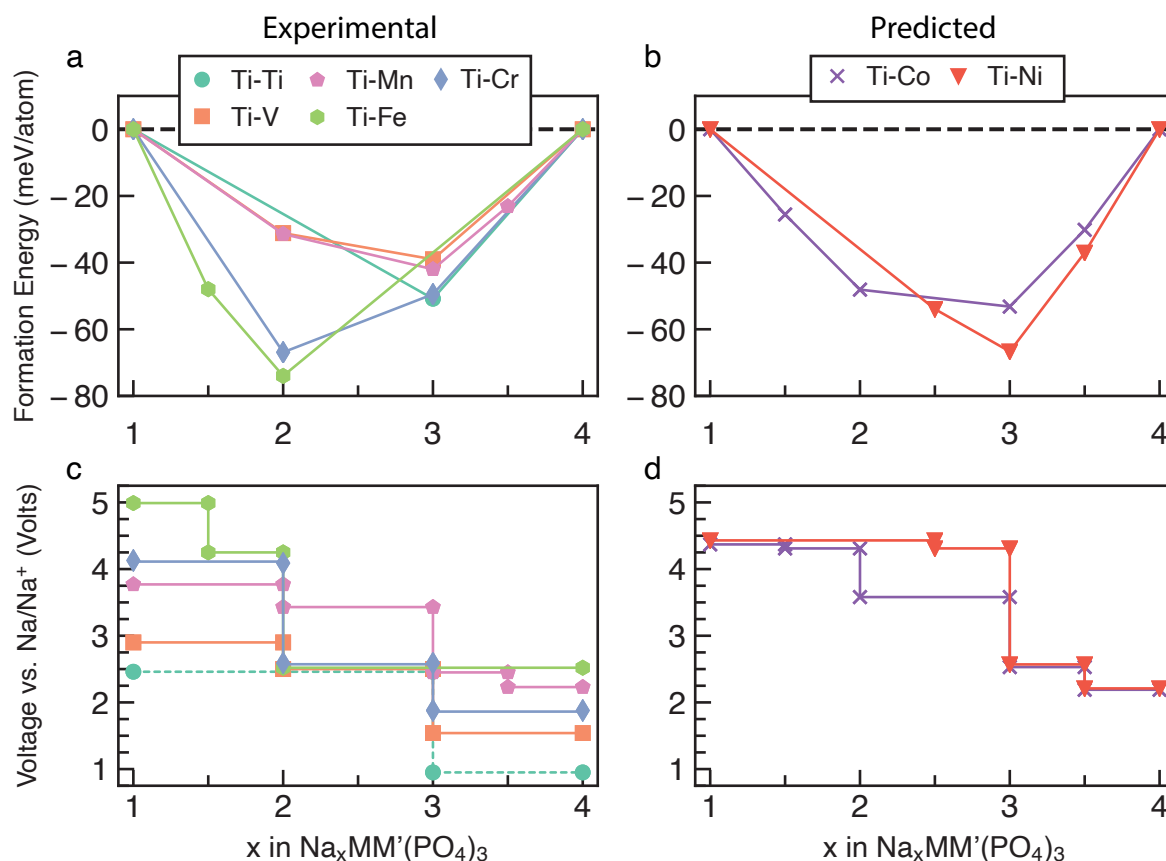


Figure 4 Panels **a** and **b** show the computed convex hulls as a function of Na concentrations (x) for $\text{Na}_x\text{TiM}'(\text{PO}_4)_3$, where $M' = \text{Ti}, \text{V}, \text{Cr}, \text{Mn}, \text{Fe}$ in panel **a** and $M' = \text{Co}$ and Ni in panel **b**. Panels **c** and **d** show the corresponding Na (de-)intercalation voltages over changes in Na-content. The energies of unstable configurations for each convex hull, as well as complete voltage curves for each compound, are given in the SI (**Figure S13 - S33**). Symbols in panels **a** and **b**, indicate stable ordered phases. To facilitate the visualization of the voltage curves near ~ 2.8 V vs. Na/Na⁺ the Ti-Cr curve in panel **c** has been slightly lifted, but it is expected to overlap the Ti-V and Ti-Mn voltage curves.

Among the $\text{Na}_x\text{TiM}'(\text{PO}_4)_3$ systems, only $\text{Na}_x\text{Ti}_2(\text{PO}_4)_3$, $\text{Na}_x\text{TiV}(\text{PO}_4)_3$ and $\text{Na}_x\text{TiMn}(\text{PO}_4)_3$ have been experimentally investigated over the entire Na composition range ($1 \leq x \leq 4$),^{[29],[51],[52],[53],[54]} while $\text{Na}_x\text{TiCr}(\text{PO}_4)_3$ ^{[55],[65]} and $\text{Na}_x\text{TiFe}(\text{PO}_4)_3$ ^[55] have been studied in limited ranges of $1 \leq x \leq 3$ and $2 \leq x \leq 4$, respectively. $\text{Na}_x\text{TiCo}(\text{PO}_4)_3$

and $\text{Na}_x\text{TiNi}(\text{PO}_4)_3$ are theoretical compounds and have not yet been reported experimentally. In general, the end member compositions at $x = 1$ and 4 (**Figures 4a** and **4b**) of the Ti-M' NaSICON electrodes adopt rhombohedral symmetry ($R\bar{3}c$ or $R\bar{3}$, or $R32$) except for $\text{Na}_4\text{Ti}^{\text{III}}\text{Cr}^{\text{II}}(\text{PO}_4)_3$ ($P\bar{1}$) and $\text{Na}_1\text{Ti}^{\text{IV}}\text{Fe}^{\text{IV}}(\text{PO}_4)_3$ ($P1$), which are theoretically derived. This could be due to Jahn-Teller effects caused by the high-spin d^4 electronic configurations of Cr^{2+} and Fe^{4+} , respectively, as well as the low stability of Fe^{4+} . For $\text{Na}_x\text{TiM}'(\text{PO}_4)_3$ with $M' = \text{V, Mn, Co and Ni}$, a global minimum in the convex hull is located at $x = 3$, and the magnitudes of the formation energy follow the trend $\text{Ni} > \text{Co} > \text{Mn} > \text{V}$. On the other hand, the global minima for the $M' = \text{Ti, Cr and Fe}$ NaSICONs are located at $x = 2$ (**Figure 4a**), which is driven by the high stability of their stable oxidation states Ti^{4+} , Cr^{3+} and Fe^{3+} , respectively. Overall, the depth of the convex hulls (i.e., maximum magnitude of formation energies) for mixed TM NaSICONs follows the trend $\text{Fe} > \text{Cr} \sim \text{Ni} > \text{Co} > \text{Ti} > \text{Mn} \sim \text{V}$.

Figures 4c and **4d** present the computed voltages for Na extraction from $\text{Na}_x\text{TiM}'(\text{PO}_4)_3$ in the composition range $1 \leq x \leq 4$. Expectedly, the compound exhibiting the lowest intercalation voltage (~ 0.96 V) is $\text{Na}_x\text{Ti}_2(\text{PO}_4)_3$ for $3 \leq x \leq 4$, which overestimates the experimental voltage (~ 0.4 V) reported by Senguttuvan et al.^[29] The DFT data of **Figure 4a** suggest that an unreported stable phase appears at $\text{Na}_{1.5}\text{TiFe}(\text{PO}_4)_3$, but with an oxidation state for Fe of 3.5 ($\text{Fe}^{\text{IV}} + \text{Fe}^{\text{III}}$). Although, the highest Na intercalation voltage (~ 4.99 V) is computed for $\text{Na}_x\text{TiFe}(\text{PO}_4)_3$ between $x = 1.5$ and $x = 1$, the oxidation state of Fe would have to be +4, which may not be experimentally accessible in a reversible manner. Furthermore, we find that

$\text{Na}_1\text{Fe}^{\text{IV}}\text{Fe}^{\text{IV}}(\text{PO}_4)_3$, where iron is expected to be Fe^{4+} appears metallic from the DOS in **Figure S10**.

To assess the quality of our computed data, we analyzed in detail the experimentally reported data for $\text{Na}_x\text{TiV}(\text{PO}_4)_3$. At $x = 1, 2$ and 4 , $\text{Na}_x\text{TiV}(\text{PO}_4)_3$ has rhombohedral symmetry ($R\bar{3}c$), while the structure of $\text{Na}_3\text{TiV}(\text{PO}_4)_3$ is monoclinic ($C2/c$).^{[51],[52]} Our calculations reproduce the rhombohedral symmetry ($R\bar{3}c$) at $x = 1$ and 4 , and the monoclinic symmetry (Cc) at $x = 3$, whereas we find a triclinic structure ($P\bar{1}$) for $\text{Na}_2\text{TiV}(\text{PO}_4)_3$.^[52] The $\text{Na}_x\text{TiV}(\text{PO}_4)_3$ convex hull (**Figure 4a**) displays a minimum at $x = 3$, analogous to the observed minima in the $\text{Na}_x\text{M}_2(\text{PO}_4)_3$ systems (**Figure 2a**); this also provides the largest step in the corresponding voltage profile of **Figure 4c**. In particular, the Na extraction from $\text{Na}_4\text{Ti}^{\text{III}}\text{V}^{\text{II}}(\text{PO}_4)_3$ takes place through the redox couples $\text{V}^{\text{III}}/\text{V}^{\text{II}}$ 1.54 V (experimentally ~ 1.6 V ^{[51],[52]}), $\text{Ti}^{\text{IV}}/\text{Ti}^{\text{III}}$ 2.50 V (~ 2.1 V), and $\text{V}^{\text{IV}}/\text{V}^{\text{III}}$ 2.90 V (~ 3.4 V) vs. Na/Na^+ , respectively. The mechanism of Na extraction from $\text{Na}_4\text{Ti}^{\text{III}}\text{V}^{\text{II}}(\text{PO}_4)_3$ has been reported to occur through a solid-solution mechanism for the $\text{V}^{\text{III}}/\text{V}^{\text{II}}$ redox couple, followed by a two-phase reaction for both the $\text{Ti}^{\text{IV}}/\text{Ti}^{\text{III}}$ and $\text{V}^{\text{IV}}/\text{V}^{\text{III}}$ redox couples.^[52]

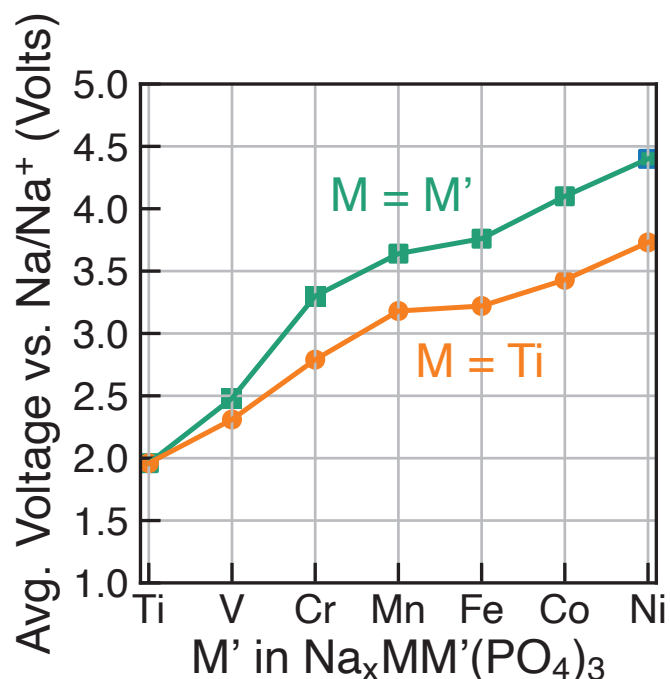


Figure 5 The calculated average voltage per extracted Na^+ ion vs. Na/Na^+ over the x range [1-4] in $\text{Na}_x\text{MM}'(\text{PO}_4)_3$ compounds, where $M = M'$ or $M = \text{Ti}$ and $M' = \text{V}, \text{Cr}, \text{Mn}, \text{Fe}, \text{Co}$ and Ni .

Due to the existence of multiple voltage steps in $\text{Na}_x\text{MM}'(\text{PO}_4)_3$ (where $M' = \text{Ti}, \text{V}, \text{Cr}, \text{Mn}, \text{Fe}, \text{Co}$ and Ni and $M = \text{Ti}$), we compare directly the computed average voltage per Na^+ exchanged over the entire composition range (i.e., $1 \leq x \leq 4$), as shown in **Figure 5**. Importantly, the overall average voltage monotonically increases from Ti to Ni in cases where $M = M'$ and $M = \text{Ti}$, which is consistent with trends in standard reduction potentials of the transition metals. We note that the M^{4+} ions, in particular, become more oxidizing as one crosses the transition series from Ti to Ni, with the lack of voltage increase from Mn to Fe reflecting the stability of their $3d^5$ configurations. Specifically, the calculated voltages increase from ~ 1.96 V (for Ti) to ~ 4.40 V vs. Na/Na^+ (for Ni) in $\text{Na}_x\text{M}_2(\text{PO}_4)_3$ (green line in **Figure 5**), while the maximum voltage is ~ 3.73 V for Ti-Ni in the case of $\text{Na}_x\text{MM}'(\text{PO}_4)_3$ ($M = \text{Ti}$) systems (orange line). Notably, the voltage values for $\text{Na}_x\text{TiM}'(\text{PO}_4)_3$ are consistently lower than in the corresponding

$\text{Na}_x\text{M}'_2(\text{PO}_4)_3$, indicating that replacing Ti with another 3d metal will always lead to an increased average voltage in both $\text{M}=\text{M}'$ and $\text{Ti}-\text{M}'$ systems.

2.4 Intercalation voltages of $\text{Na}_x\text{MM}'(\text{PO}_4)_3$

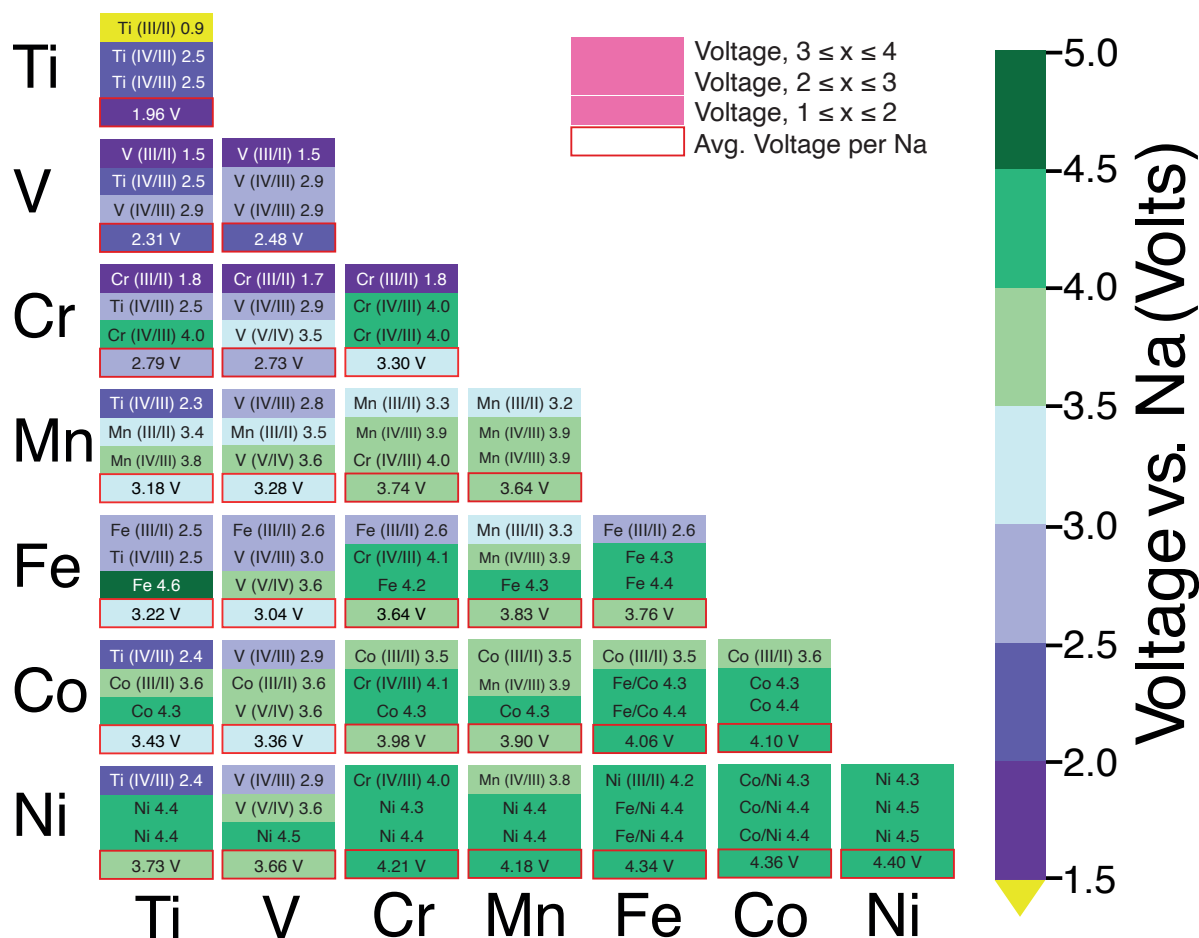


Figure 6 A voltage map derived from our calculations of 3d NaSICON electrodes, $\text{Na}_x\text{MM}'(\text{PO}_4)_3$, where M and $\text{M}' = \text{Ti}, \text{V}, \text{Cr}, \text{Mn}, \text{Fe}, \text{Co}$ and Ni . The text in each box represents the redox pair and the corresponding voltage vs. Na/Na^+ (given by the color bar). The color of text in the sub-boxes (black or white) does not have any physical significance other than to enhance the visibility of the plot. The color fill in each sub-box represents the voltage from the scale given on right. The red-outlined bottom sub-box reflects the average voltage per Na in the overall range of $1 \leq x \leq 4$.

Figure 6 consolidates the computed voltages of 28 plausible combinations of 3d transition metals in $\text{Na}_x\text{MM}'(\text{PO}_4)_3$ with M and M' in a 1:1 ratio. In **Figure 6**, boxes outlined in red represent the average voltage per extracted Na in the entire $1 \leq x \leq 4$ concentration range for each combination of transition metals. The NaSICON systems investigated cover a range of average voltages from ~ 1.96 to ~ 4.4 V vs. Na/Na⁺. Redox couples are indicated in each box whenever we could identify the appropriate oxidation states as described in **Section 2.2**. The diagonal of **Figure 6** displays the single-transition-metal NaSICONs (M = M'), whose average voltages map directly to **Figure 5**. Notably, the highest average voltages of ~ 4.3 – 4.4 V are attained by the theoretical $\text{Na}_x\text{Ni}_2(\text{PO}_4)_3$, $\text{Na}_x\text{CoNi}(\text{PO}_4)_3$ and $\text{Na}_x\text{FeNi}(\text{PO}_4)_3$ compounds. In general, voltages in NaSICONs are set by the redox couples M^{III}/M^{II} and M^{IV}/M^{III} but notable exceptions to this trend are for V and Nb-based NaSICONs, which can also operate on the V^V/V^{IV} couple (see mixed $\text{Na}_x\text{VM}'(\text{PO}_4)_3$ systems in **Figure 6**) and the Nb^V/Nb^{IV} couple in $\text{Na}_x\text{NbTi}(\text{PO}_4)_3$ not discussed here.^[66]

2.5 Thermodynamic stabilities of selected $\text{Na}_x\text{M}_2(\text{PO}_4)_3$ compounds

The calculated quaternary phase diagrams for the systems Na-P-O-Mn, Na-P-O-Co, and Na-P-O-Ni (**Figures 7** and **S34** in SI) reflect the stabilities of the as-yet-unreported $\text{Na}_x\text{M}_2(\text{PO}_4)_3$ compounds with these transition metals compared with the stable elemental, binary, ternary and quaternary phases. While it remains extremely challenging to characterize quaternary (and beyond) phase diagrams solely based on sparse experimental data, theory provides a viable alternative for investigating such

complex systems. We calculated all the elements and binary/ternary/quaternary compounds available in the inorganic crystal structure database (ICSD)^[67] within the Na-P-O-Mn, -Co and -Ni quaternary systems.

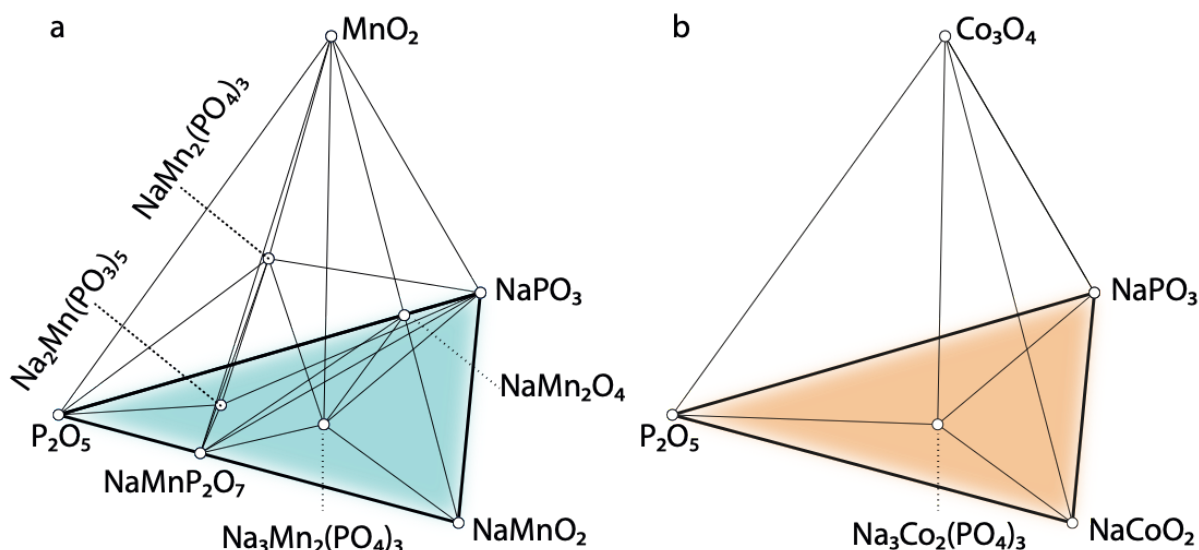


Figure 7 Panels **a** and **b** show portions of the computed phase diagrams of Na-P-O-Mn and Na-P-O-Co at 0 K. Two stable NaSICON structures with formulae $\text{NaMn}_2(\text{PO}_4)_3$ and $\text{Na}_3\text{Mn}_2(\text{PO}_4)_3$ are observed in the phase diagram of Na-P-O-Mn, which are in equilibrium with the highly stable binary (P_2O_5 and MnO_2) and ternary (NaMnO_2 and NaPO_3) compounds. In panel **b**, a stable NaSICON structure of formula $\text{Na}_3\text{Co}_2(\text{PO}_4)_3$ is observed in the phase diagram of Na-P-O-Co, which is in equilibrium with the highly stable binary (P_2O_5 and Co_3O_4) and ternary (NaCoO_2 and NaPO_3) compounds.

Figure 7a shows the computed phase diagram of the Na-P-O-Mn system, where the open circles correspond to stable phases in the global phase diagrams and the black lines show the equilibria among various compounds. The computed phase diagram of Na-Mn-P-O shows that $\text{Na}_3\text{Mn}^{\text{III}}\text{Mn}^{\text{III}}(\text{PO}_4)_3$ and $\text{Na}_1\text{Mn}^{\text{IV}}\text{Mn}^{\text{IV}}(\text{PO}_4)_3$ are stable compounds. $\text{Na}_3\text{Mn}^{\text{III}}\text{Mn}^{\text{III}}(\text{PO}_4)_3$ has the structure of the monoclinic (Cc) polymorph, whereas $\text{Na}_1\text{Mn}^{\text{IV}}\text{Mn}^{\text{IV}}(\text{PO}_4)_3$ has a rhombohedral ($R\bar{3}$) structure. From our computations, we observed a Jahn-Teller distortion driven by the $\text{Mn}^{3+} 3d^4$ ions and highlighted by four longer equatorial bonds $\sim 2.10 \text{ \AA}$ and two shorter axial bonds of

~1.96 Å, respectively. No Ni-containing NaSICON phases appear stable in the Na-Ni-P-O system (**Figure S34**). In the Na-Co-P-O phase diagram (**Figure 7b**), only $\text{Na}_3\text{Co}^{\text{III}}\text{Co}^{\text{III}}(\text{PO}_4)_3$ appears stable and exhibits rhombohedral symmetry ($R\bar{3}$). From this analysis, it is predicted that $\text{Na}_3\text{Mn}^{\text{III}}\text{Mn}^{\text{III}}(\text{PO}_4)_3$, $\text{Na}_1\text{Mn}^{\text{IV}}\text{Mn}^{\text{IV}}(\text{PO}_4)_3$, and $\text{Na}_3\text{Co}^{\text{III}}\text{Co}^{\text{III}}(\text{PO}_4)_3$ have potential for successful experimental synthesis, given their thermodynamic stabilities.

3. Discussion

Using first-principles calculations, we investigated the electrochemical properties of 28 distinct transition-metal-based NaSICONs as positive electrode materials for NIBs. The NaSICONs considered included both single-transition-metal $\text{Na}_x\text{M}_2(\text{PO}_4)_3$ as well as mixed-transition-metal, $\text{Na}_x\text{MM}'(\text{PO}_4)_3$, with M, M' = Ti, V, Cr, Mn, Fe, Co and Ni. To guide our discussion, we summarize the reported experimental voltages and experimental gravimetric as well as theoretical gravimetric capacities of some $\text{Na}_x\text{MM}'(\text{PO}_4)_3$ systems in **Table I**. For a transparent and fair comparison between theoretical and experimentally reported capacities in **Table I**, the reported capacities are renormalized from the reported composition (pristine) to the molecular weight of the $\text{Na}_4\text{MM}'(\text{PO}_3)_4$. The theoretical capacities are also computed with respect to the $\text{Na}_4\text{MM}'(\text{PO}_3)_4$ compounds.

Table I Experimentally observed $\text{Na}_x\text{MM}'(\text{PO}_4)_3$ phases along with the corresponding Na concentrations, structures, Na^+ reversible intercalation voltages, redox couples, mechanism of Na^+ intercalation, and gravimetric capacities. The intercalation voltages (in V) and theoretical (Theo.) capacities (in mAh/g) are shown. Rev. and Irrev. indicate experimentally reversible and irreversible processes. ? is used whenever the space group of a specific phase is unknown or not reported. Intercalation voltages account for the number of Na^+ ions exchanged. Whenever available, the space group of each phase is reported. For a transparent comparison between theoretical and experimentally reported capacities, the reported capacities are renormalized to the molecular weight of $\text{Na}_4\text{MM}'(\text{PO}_3)_4$. The theoretical capacities (Theo.) are also computed with respect to the $\text{Na}_4\text{MM}'(\text{PO}_3)_4$ compound.

M-M' (M=M')	x = 1	2	3	4	Reported Capacity	Theo. Capacity
Ti-Ti ^[29]	? 	2.1 V, $\text{Ti}^{\text{IV}}/\text{Ti}^{\text{III}}$, Rev.	P-1 	R-3c 0.4 V, $\text{Ti}^{\text{III}}/\text{Ti}^{\text{II}}$, Irrev.	142.7	170.1
V-V ^[38,39,41,61]	R-3c 	3.4 V, $\text{V}^{\text{V}}/\text{V}^{\text{III}}$, Rev.	C2/c 	R-3c 1.6 V, $\text{V}^{\text{III}}/\text{V}^{\text{II}}$, Irrev.	156.7	167.9
Cr-Cr ^[49]	R-3c 	4.5 V, $\text{Cr}^{\text{IV}}/\text{Cr}^{\text{III}}$, Rev.	R-3c 		93.3	111.5
Fe-Fe ^[47,48]	? 	3.4 V, $\text{Fe}^{\text{IV}}/\text{Fe}^{\text{III}}$, Rev.	C2/c 	R-3c 2.5 V, $\text{Fe}^{\text{III}}/\text{Fe}^{\text{II}}$, Rev.	85.8	164.6
M-M'	x = 1	2	3	4	Reported Capacity	Theo. Capacity
Ti-V ^[51,52]	R-3c 3.4 V, $\text{V}^{\text{IV}}/\text{V}^{\text{III}}$, Rev.	R-3c 2.1 V, $\text{Ti}^{\text{IV}}/\text{Ti}^{\text{III}}$, Rev.	C2/c 1.6 V, $\text{V}^{\text{III}}/\text{V}^{\text{II}}$, Rev.	R-3c 	132.8	169.0
Ti-Cr ^[55]	R-3c 4.5 V, $\text{Cr}^{\text{IV}}/\text{Cr}^{\text{III}}$, Rev.	R-3c 2.1 V, $\text{Ti}^{\text{IV}}/\text{Ti}^{\text{III}}$, Rev.	R-3c 		–	112.4
Ti-Mn ^[53,54]	R-3c 4. V, $\text{Mn}^{\text{IV}}/\text{Mn}^{\text{III}}$, Rev.	R-3c 3.5 V, $\text{Mn}^{\text{III}}/\text{Mn}^{\text{II}}$, Rev.	R-3c 2.1 V, $\text{Ti}^{\text{IV}}/\text{Ti}^{\text{III}}$, Rev.	? 	152.3	167.6
Ti-Fe ^[55]		R-3c 2.4 V, $\text{Fe}^{\text{III}}/\text{Fe}^{\text{II}}$, Rev.	R-3c 2.1 V, $\text{Ti}^{\text{IV}}/\text{Ti}^{\text{III}}$, Rev.	R-3c 	–	111.5
V-Cr ^[50]	? 4.1 V, $\text{V}^{\text{V}}/\text{V}^{\text{IV}}$, Rev.	? 3.4 V, $\text{V}^{\text{IV}}/\text{V}^{\text{III}}$, Rev.	R-3c 		85.7	111.7
V-Mn ^[35,68]	R-3c 3.9 V, $\text{V}^{\text{V}}/\text{V}^{\text{IV}}$, Irrev.	R-3c 3.6 V, $\text{Mn}^{\text{III}}/\text{Mn}^{\text{II}}$, Rev.	R-3c 3.4 V, $\text{V}^{\text{IV}}/\text{V}^{\text{III}}$, Rev.	R-3c 	156.0	166.6
V-Fe ^[30,36]		? 3.3 V, $\text{V}^{\text{IV}}/\text{V}^{\text{III}}$, Rev.	C2/c 2.5 V, $\text{Fe}^{\text{III}}/\text{Fe}^{\text{II}}$, Rev.	? 	98.1	110.8
V-Ni ^[36]		? 3.9 V, $\text{V}^{\text{V}}/\text{V}^{\text{IV}}:\text{Ni}^{\text{III}}/\text{Ni}^{\text{II}}$, Rev.	? 3.5 V, $\text{V}^{\text{IV}}/\text{V}^{\text{III}}$, Rev.	R-3c 	80.0	110.2
Cr-Mn ^[31,37]	R-3c 4.4 V, $\text{Cr}^{\text{IV}}/\text{Cr}^{\text{III}}$, Rev.	R-3c 4.2 V, $\text{Mn}^{\text{IV}}/\text{Mn}^{\text{III}}$, Rev.	R-3c 3.6 V, $\text{Mn}^{\text{III}}/\text{Mn}^{\text{II}}$, Rev.	R-3c 	160.5	166.2

Among the $\text{Na}_x\text{M}_2(\text{PO}_4)_3$ compounds, $\text{Na}_x\text{Cr}_2(\text{PO}_4)_3$ delivers the highest measured voltage of ~4.5 V (~4 V calculated theoretically) vs. Na/Na^+ ,^[49] albeit with a limited

capacity of just ~ 98 mAh/g, and corresponding to the extraction of 2 Na from $\text{Na}_3\text{Cr}^{\text{III}}\text{Cr}^{\text{III}}(\text{PO}_4)_3$ to form $\text{Na}_1\text{Cr}^{\text{IV}}\text{Cr}^{\text{III}}(\text{PO}_4)_3$. Indeed, $\text{Na}_4\text{Cr}_2(\text{PO}_4)_3$ has not yet been obtained by either a chemical or an electrochemical process. $\text{Na}_4\text{Cr}^{\text{III}}\text{Cr}^{\text{II}}(\text{PO}_4)_3$ would require Cr to exist in a mixed, $\text{Cr}^{\text{III}}/\text{Cr}^{\text{II}}$ oxidation state, with Cr^{2+} (high-spin d^4) being typically an unstable oxidation state for Cr and easily prone to Jahn-Teller distortions in octahedral environments, such as in NaSICON.^[69]

$\text{Na}_x\text{V}_2(\text{PO}_4)_3$ (NVP) exhibits the second highest measured voltage among the single transition metal NaSICONs, with a computed average voltage of ~ 2.48 V vs. Na/Na^+ (**Figure 5**). With the same number of maximum electrons exchanged in $\text{Na}_x\text{M}_2(\text{PO}_4)_3$ (where $\text{M} = \text{Ti}$ or V), and Ti being lighter than V , $\text{Na}_x\text{Ti}_2(\text{PO}_4)_3$ is expected to show the largest gravimetric capacity (see **Table I**). $\text{Na}_x\text{Ti}_2(\text{PO}_4)_3$ and NVP provide the largest theoretical gravimetric capacities (~ 170.1 mAh/g and ~ 167.9 mAh/g for $\text{Na}_4\text{M}_2(\text{PO}_4)_3$, see **Table I**) reported in single transition metal NaSICONs. In theory, additional capacity and an increased voltage could be achieved by exploiting the $\text{V}^{\text{V}}/\text{V}^{\text{IV}}$ redox couple in the reaction $\text{Na}_1\text{V}^{\text{V}}\text{V}^{\text{IV}}(\text{PO}_4)_3 \rightarrow \text{Na}^+ + 1\text{e}^- \text{V}^{\text{V}}\text{V}^{\text{IV}}(\text{PO}_4)_3$. While the seminal report by Gopalakrishnan *et al.* suggested the possibility of chemically extracting the last Na^+ ion to form $\text{V}^{\text{V}}\text{V}^{\text{IV}}(\text{PO}_4)_3$,^[70] subsequent attempts to do so have proven unsuccessful. Note that thermodynamically, $\text{V}^{\text{V}}\text{V}^{\text{IV}}(\text{PO}_4)_3$ is not a stable compound^[71] and is predicted to decompose into $\text{VPO}_5 + \text{VP}_2\text{O}_7$.

We assessed the existence of uncharted single-transition-metal NaSICONs, which are Ni, Co and Mn. Except for $\text{Na}_1\text{Mn}^{\text{IV}}\text{Mn}^{\text{IV}}(\text{PO}_4)_3$, $\text{Na}_3\text{Mn}^{\text{III}}\text{Mn}^{\text{III}}(\text{PO}_4)_3$ and $\text{Na}_3\text{Co}^{\text{III}}\text{Co}^{\text{III}}(\text{PO}_4)_3$ which appear stable according to our computed convex hulls but

have not been reported experimentally, our analysis of the phase diagrams indicates that Ni-, and Co- NaSICONs are generally unstable. However, Mn has been mixed effectively with Ti, V and Cr, while Ni-V mixed NaSICONs have also been made (**Table I**).^[35] In particular, Zhou *et al.*^[36] and later Chen and collaborators^[35] have synthesized Mn^{II}-containing Na₄Mn^{II}V^{III}(PO₄)₃, which upon Na extraction exploits the Mn^{III}/Mn^{II} redox couple, where Mn³⁺ 3d⁴ is Jahn-Teller active.

In the case of mixed Na₄MM'(PO₄)₃ NaSICONs, we kept the M:M' ratio to 1:1 (otherwise too many number of cases). From an extensive assessment of polyanion-based electrodes, Masquelier and Croguennec^[18] observed that the redox potentials of specific transition metals remain nearly independent^[1] from those of other transition metals that may be present. This general rule is also well supported by the simulations that are summarized in **Figure 6**. Based on this general principle, one can envision selected combinations of transition metals delivering reversible high voltages vs. Na/Na⁺. For example, the Ti^{IV}/Ti^{III} redox couple showed a similar voltage^[18] (~2.1 V vs. Na/Na⁺) in three related NaSICONs systems: Na_xTi₂(PO₄)₃, Na_xTiNb(PO₄)₃ and Na_xTiFe(PO₄)₃, respectively. Notably, in experiments, there is a consistent shift of 0.3 V between the voltages measured vs. Na/Na⁺ compared to those measured vs. Li/Li⁺).

The Na_xTiV(PO₄)₃ system has been shown to provide the largest gravimetric capacity (~187.1 mAh/g, **Table I**) among NaSICONs as a result of the accessibility of V^{IV}/V^{III}/V^{II} and Ti^{IV}/Ti^{III} redox couples. Nevertheless, the computed average voltage (~2.3 V, **Figure 6**) of Na_xTiV(PO₄)₃ highlights the low energy density of the

system.^{[51],[52]} More promising in terms of overall capacities and voltages, and thus energy density, are $\text{Na}_x\text{TiCr}(\text{PO}_4)_3$,^{[55],[65]} $\text{Na}_x\text{TiMn}(\text{PO}_4)_3$,^{[53],[54]} $\text{Na}_x\text{CrMn}(\text{PO}_4)_3$,^{[31],[37]} $\text{Na}_x\text{VCr}(\text{PO}_4)_3$,^[50] and $\text{Na}_x\text{VMn}(\text{PO}_4)_3$,^[35] but the reversible extraction/insertion of Na from some of these systems remains to be verified. Excluding some specific exceptions, especially Fe, Co and Ni based NaSICONs since they appear metallic, our simulations are also able to capture the mechanism of Na intercalation in mixed NaSICON electrodes. For example, $\text{Na}_3\text{VFe}(\text{PO}_4)_3$ has been reported to reversibly insert Na with the activation of the $\text{Fe}^{\text{III}}/\text{Fe}^{\text{II}}$ and $\text{V}^{\text{III}}/\text{V}^{\text{II}}$ redox couples, respectively (see **Table I**),^[36] and this behavior is reproduced by our calculations (**Figure 6** and **Figure S21** of SI). Similar conclusions can be advanced for mixed TiV, TiCr, VCr and CrMn NaSICON materials.

From our analysis (**Figure 6**), specific unexplored combinations of transition metals appear to be worthy of future study. Our calculations suggest promising NaSICON compositions in terms of average voltages, such as TiCo, VCo, CrFe and CrCo NaSICONs as reported in **Figure 5** and **Table 1**. Both CrFe and CrCo NaSICONs are predicted to exploit the high voltage $\text{Cr}^{\text{IV}}/\text{Cr}^{\text{III}}$ redox couple, which has been proven effective into other mixed NaSICONs, e.g. TiCr, VCr and MnCr.^{[65],[50]} Although the addition of Co into Ti, V and Cr appears interesting, our analysis of the $\text{Na}_x\text{Co}_2(\text{PO}_4)_3$ system suggests that only $\text{Na}_3\text{Co}^{\text{III}}\text{Co}^{\text{III}}(\text{PO}_4)_3$ with $\text{Co}^{3+} 3d^6$ (low spin) is thermodynamically stable, but this compound has not been yet synthesized. While one would target compounds with Co^{2+} to ensure high voltages, it appears possible to introduce Co in smaller proportions^[72] than a 1:1 ratio, but more experimental and theoretical work is required.

We do not anticipate Ni to be of importance in mixed NaSICON systems due to the high instability of quaternary $\text{Na}_x\text{Ni}_2(\text{PO}_4)_3$. Notably, Manoun *et al.*^[73] have briefly reported the synthesis of $\text{Na}_4\text{Cr}^{\text{III}}\text{Ni}^{\text{II}}(\text{PO}_4)_3$. Indeed, a recent report by Zhou *et al.*^[36] claims the extraction of Na from $\text{Na}_x\text{VNi}(\text{PO}_4)_3$ (**Table I**) involving the redox couples $\text{V}^{\text{IV}}/\text{V}^{\text{III}}$, $\text{V}^{\text{V}}/\text{V}^{\text{IV}}$, and $\text{Ni}^{\text{III}}/\text{Ni}^{\text{II}}$. Nevertheless, we speculate that the Ni content of the materials is not in a 1:1 ratio but appears to be significantly lower. Furthermore, the highest voltage accessed (<4.3 V vs. Na/Na^+) during the electrochemical cycling is lower than that of the expected Ni redox couple. While our DFT calculations seem to verify the activity of the $\text{V}^{\text{IV}}/\text{V}^{\text{III}}$ and $\text{V}^{\text{V}}/\text{V}^{\text{IV}}$ redox couples in $\text{Na}_x\text{VNi}(\text{PO}_4)_3$ (**Figure 6**), we are unable to verify the oxidation states involved in the $\text{Ni}^{\text{III}}/\text{Ni}^{\text{II}}$ reaction from the computed magnetic moments as the material becomes metallic in our simulations (**Figure S12**). Our findings also cast doubt on the activity of Ni in this compound as reflected by the limited gravimetric capacity reported experimentally (~ 80 mAh/g).^[36]

4. Conclusions

Using *ab initio* density functional theory and thermodynamics, we explored the full chemical map of 3d transition metal-based NaSICON phosphates $\text{Na}_x\text{MM}'(\text{PO}_4)_3$ (M, M' = Ti, V, Cr, Mn, Fe, Co and Ni) positive electrode materials for high-energy density and safe sodium-ion batteries. We calculated the ground state structures at various Na contents as well as the corresponding Na-intercalation voltages and redox processes for 28 distinct NaSICON compositions of which only 13 have been reported experimentally.

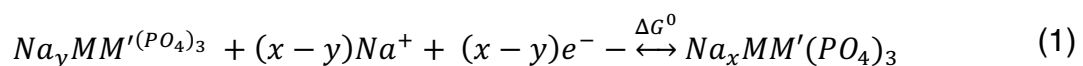
Further, we investigated the Na-intercalation properties of previously unreported $\text{Na}_x\text{Mn}_2(\text{PO}_4)_3$ and $\text{Na}_x\text{VCo}(\text{PO}_4)_3$ ($1 \leq x \leq 4$), among others. The calculated quaternary phase diagrams of the Na-P-O-M (M= Mn, Co and Ni) chemical systems indicate the instability of Ni and most Co-based NaSICONs, though the $\text{Na}_1\text{Mn}^{\text{IV}}\text{Mn}^{\text{IV}}(\text{PO}_4)_3$, $\text{Na}_3\text{Mn}^{\text{III}}\text{Mn}^{\text{III}}(\text{PO}_4)_3$ and $\text{Na}_3\text{Co}^{\text{III}}\text{Co}^{\text{III}}(\text{PO}_4)_3$ compounds are identified as stable compositions. We performed a complete analysis of the wide-ranging chemical space of NaSICON phosphate cathode materials for Na-ion batteries, and our work can be used to guide further experimental synthesis of the new and promising compositions identified here.

5. Methodology

We used the Vienna ab initio simulation package (VASP)^{[74],[75]} for *ab initio* density functional theory (DFT) total energy calculations. The projector augmented wave (PAW) potentials were used for the core wave-functions. The Perdew–Burke–Ernzerhof (PBE) parameterized spin-polarized generalized gradient approximation (GGA) was used for the exchange and correlation energy.^[76] The strong on-site coulomb correlation of *3d* electrons of the transition metals (Ti, V, Cr, Mn, Fe, Co and Ni) is addressed with Hubbard's *U* correction^[77] according to the Dudarev method.^[78] The effective *U* parameters used are 4.0 eV for Ti, 3.1 for V, 3.5 for Cr, 3.9 for Mn, 4.0 for Fe, 3.4 for Co, and 6.0 for Ni.^[79] We also introduced an empirical correction of 1.36 eV/O₂^[80] to remedy the spurious error originating from the well-known overbinding of O₂ while using GGA.

The periodic wave functions were expanded in terms of plane waves up to a kinetic energy cut-off of 520 eV. The PAW potentials used to describe the core electrons were Na 08Apr2002 3s¹, P 17Jan2003 2s²3p³, O 08Apr2002 2s²2p⁴, Ti 08Apr2002 3d³4s¹, V_pv 07Sep2000 3p⁶3d⁴4s¹, Cr 06Sep2000 3d⁵4s¹, Mn 06Sep2000 3d⁶4s¹, Fe 06Sep2000 3d⁷4s¹, Co 06Sep2000 3d⁸4s¹, and Ni 06Sep2000 3d⁹4s¹. Additionally, a Γ -centred Monkhorst-Pack^[81] k -point mesh with 25 subdivisions along each reciprocal lattice vector was applied to all structures. Using these settings, the total energy of each structure was converged to within 10⁻⁵ eV/cell, atomic forces within 10⁻² eV/Å and the stress within 0.29 GPa.

An intercalation battery based on the NaSICON positive electrodes implies the reversible insertion/extraction of Na⁺-ions into/from the Na_yMM'(PO₄)₃ framework according to the redox reaction of **Equation 1**.



where y and x are the initial and final Na concentration in NaSICON framework and ΔG^0 is the change of Gibbs energy at 0K for the reaction of **Equation 1**. Here, we approximated the Gibbs energy of each component by the DFT total energies (i.e., $G \approx E$), thus neglecting the pV and entropic contributions. The average voltage across an intercalation extent $(x - y)$ can be calculated from the ΔG^0 , as in **Equation 2**.

$$V = -\frac{\Delta G^0}{(x-y)F} \sim \frac{E(\text{Na}_x\text{MM}'(\text{PO}_4)_3) - [E(\text{Na}_y\text{MM}'(\text{PO}_4)_3) + (x-y)\mu_{\text{Na}}]}{(x-y)F} \quad (2)$$

where μ_{Na} is the Na chemical potential (set to bulk Na metal here) and F is the Faraday constant.

To establish the general phase behavior of Na (de)intercalation into the $\text{Na}_y\text{MM}'(\text{PO}_4)_3$ structure, we monitored, using **Equation 3**, the formation energies ($E_f(x)$) of various orderings at different Na concentrations, x ($1 \leq x \leq 4$), with respect to the DFT energies of the fully discharged (i.e., $E[\text{Na}_4\text{MM}'(\text{PO}_4)_3]$), and fully charged ($E[\text{NaMM}'(\text{PO}_4)_3]$) configurations.

$$E_f(x) = E[\text{Na}_x\text{MM}'(\text{PO}_4)_3] - \left(\frac{4-x}{3}\right)E[\text{Na}_1\text{MM}'(\text{PO}_4)_3] - \left(\frac{x-1}{3}\right)E[\text{Na}_4\text{MM}'(\text{PO}_4)_3] \quad (3)$$

Different NaSICON structures were studied according to specific Na concentrations in $\text{Na}_x\text{MM}'(\text{PO}_4)_3$ with M and M' = Ti, V, Cr, Mn, Fe, Co, and Ni. In choosing the amount of mixing of TM in these NaSICON structures, we have considered only two distinct situations: i) $M = M'$, which leads to $\text{Na}_x\text{M}_2(\text{PO}_4)_3$, and ii) M and M' in the ratio 1:1.

When fully sodiated, the fully ordered rhombohedral symmetry ($R\bar{3}c$) of the high temperature NaSICON structure is typically observed (e.g., $\text{Na}_4\text{Fe}^{\text{III}}\text{Fe}^{\text{II}}(\text{PO}_4)_3$ ^[60]) and is therefore our starting model to study Na removal and TM mixing. Na vacancies are created in the fully sodiated structure ($\text{Na}_4\text{MM}'(\text{PO}_4)_3$), resulting in $\text{Na}_x\text{MM}'(\text{PO}_4)_3$,

where the Na content varies in the range $1 \leq x \leq 4$ in steps of $\Delta x = 0.5$. The possible configurations originating from the various orderings of Na and vacancies (Va) in the NaSICON are obtained using the pymatgen library.^[82] A ranking according to the classical Ewald energy^[83] based on integer charges (i.e., Na=+1, P=+5, O=-2) and variable charge on the transition metal (+2, +3, +4) is applied to limit the number of possible structures to a computationally tractable level. For mixed transition metal NaSICONs, the ordering of M and M' is simultaneously performed with that of Na and Va. DFT calculations are performed on the primitive cell and supercells ($2 \times 1 \times 1$) of these orderings. A formula unit of the fully discharged NaSICON ($\text{Na}_4\text{MM}'(\text{PO}_4)_3$) contains 21 atoms.

Acknowledgements

P. C., C. M., A. K. C., and J.-N. C. are grateful to the ANR-NRF NRF2019-NRF-ANR073 Na-MASTER. P.C. and B. S acknowledge funding from the National Research Foundation under his NRF Fellowship NRFF12-2020-0012. L. C., D. C. and C. M. acknowledge the ANRT and TIAMAT for the funding of S. P.'s PhD thesis as well as the financial support of Région Nouvelle Aquitaine and of the French National Research Agency (STORE-EX Labex Project ANR-10-LABX-76-01). The computational work was performed on resources of the National Supercomputing Centre, Singapore (<https://www.nscg.sg>).

References

- [1] A. K. Padhi, K. S. Nanjundaswamy, C. Masquelier, J. B. Goodenough, *J. Electrochem. Soc.* **1997**, *144*, 2581.
- [2] A. Manthiram, J. B. Goodenough, *J. Solid State Chem.* **1987**, *71*, 349.
- [3] A. K. Padhi, V. Manivannan, J. B. Goodenough, *J. Electrochem. Soc.* **1998**, *145*, 1518.
- [4] B. Nykvist, M. Nilsson, *Nat. Clim. Chang.* **2015**, *5*, 329.
- [5] O. Schmidt, A. Hawkes, A. Gambhir, I. Staffell, *Nat. Energy* **2017**, *2*, 1.
- [6] E. A. Olivetti, G. Ceder, G. G. Gaustad, X. Fu, *Joule* **2017**, *1*, 229.
- [7] J. M. Tarascon, *Nat. Chem.* **2010**, *2*, 510.
- [8] D. Larcher, J. M. Tarascon, *Nat. Chem.* **2015**, *7*, 19.
- [9] S. W. Kim, D. H. Seo, X. Ma, G. Ceder, K. Kang, *Adv. Energy Mater.* **2012**, *2*, 710.
- [10] V. Palomares, P. Serras, I. Villaluenga, K. B. Hueso, J. Carretero-González, T. Rojo, *Energy Environ. Sci.* **2012**, *5*, 5884.
- [11] N. Yabuuchi, K. Kubota, M. Dahbi, S. Komaba, *Chem. Rev.* **2014**, *114*, 11636.
- [12] I. Hasa, S. Mariyappan, D. Saurel, P. Adelhelm, A. Y. Kuposov, C. Masquelier, L. Croguennec, M. Casas-Cabanas, *J. Power Sources* **2021**, *482*, 228872.
- [13] S. H. Bo, X. Li, A. J. Toumar, G. Ceder, *Chem. Mater.* **2016**, *28*, 1419.
- [14] J.-M. Tarascon, *Joule* **2020**, DOI 10.1016/j.joule.2020.06.003.
- [15] K. Kubota, T. Asari, H. Yoshida, N. Yabuuchi, H. Shiiba, M. Nakayama, S. Komaba, *Adv. Funct. Mater.* **2016**, *26*, 6047.
- [16] P. F. Wang, Y. You, Y. X. Yin, Y. G. Guo, *Adv. Energy Mater.* **2018**, *8*, DOI 10.1002/aenm.201701912.
- [17] T. Jin, H. Li, K. Zhu, P. F. Wang, P. Liu, L. Jiao, *Chem. Soc. Rev.* **2020**, *49*, 2342.
- [18] C. Masquelier, L. Croguennec, *Chem. Rev.* **2013**, *113*, 6552.
- [19] S. C. Chung, J. Ming, L. Lander, J. Lu, A. Yamada, *J. Mater. Chem. A* **2018**, *6*, 3919.
- [20] P. Barpanda, G. Oyama, S. Nishimura, S.-C. Chung, A. Yamada, *Nat. Commun.* **2014**, *5*, 4358.
- [21] H. Y. P. Hong, *Mater. Res. Bull.* **1976**, *11*, 173.
- [22] J. B. Goodenough, H. Y. P. Hong, J. A. Kafalas, *Mater. Res. Bull.* **1976**, *11*, 203.
- [23] Q. Ma, C. L. Tsai, X. K. Wei, M. Heggen, F. Tietz, J. T. S. Irvine, *J. Mater. Chem. A* **2019**, *7*, 7766.
- [24] Z. Jian, Y. S. Hu, X. Ji, W. Chen, *Adv. Mater.* **2017**, *29*, DOI 10.1002/adma.201601925.
- [25] R. V. Panin, O. A. Drozhzhin, S. S. Fedotov, N. R. Khasanova, E. V. Antipov, *Electrochim. Acta* **2018**, *289*, 168.
- [26] C. Delmas, F. Cherkaoui, A. Nadiri, P. Hagenmuller, *Mater. Res. Bull.* **1987**, *22*, 631.
- [27] C. Delmas, A. Nadiri, J. L. Soubeyroux, *Solid State Ionics* **1988**, *28–30*, 419.
- [28] X. Zhang, X. Rui, D. Chen, H. Tan, D. Yang, S. Huang, Y. Yu, *Nanoscale* **2019**, *11*, 2556.
- [29] P. Senguttuvan, G. Rouse, M. E. Arroyo y de Dompablo, H. Vezin, J.-M.

- Tarascon, M. R. Palacín, *J. Am. Chem. Soc.* **2013**, *135*, 3897.
- [30] B. M. de Boisse, J. Ming, S. Nishimura, A. Yamada, *J. Electrochem. Soc.* **2016**, *163*, A1469.
- [31] J. Wang, Y. Wang, D. Seo, T. Shi, S. Chen, Y. Tian, H. Kim, G. Ceder, *Adv. Energy Mater.* **2020**, *10*, 1903968.
- [32] D. A. Stevens, J. R. Dahn, *J. Electrochem. Soc.* **2000**, *147*, 1271.
- [33] M. Dahbi, M. Kiso, K. Kubota, T. Horiba, T. Chafik, K. Hida, T. Matsuyama, S. Komaba, *J. Mater. Chem. A* **2017**, *5*, 9917.
- [34] H. Kim, J. Hong, G. Yoon, H. Kim, K.-Y. Park, M.-S. Park, W.-S. Yoon, K. Kang, *Energy Environ. Sci.* **2015**, *8*, 2963.
- [35] F. Chen, V. M. Kovrugin, R. David, O. Mentré, F. Fauth, J. Chotard, C. Masquelier, *Small Methods* **2019**, *3*, 1800218.
- [36] W. Zhou, L. Xue, X. Lü, H. Gao, Y. Li, S. Xin, G. Fu, Z. Cui, Y. Zhu, J. B. Goodenough, *Nano Lett.* **2016**, *16*, 7836.
- [37] W. Zhang, H. Li, Z. Zhang, M. Xu, Y. Lai, S. L. Chou, *Small* **2020**, DOI 10.1002/sml.202001524.
- [38] X. Yao, Z. Zhu, Q. Li, X. Wang, X. Xu, J. Meng, W. Ren, X. Zhang, Y. Huang, L. Mai, *ACS Appl. Mater. Interfaces* **2018**, *10*, 10022.
- [39] K. Saravanan, C. W. Mason, A. Rudola, K. H. Wong, P. Balaya, *Adv. Energy Mater.* **2013**, *3*, 444.
- [40] Y. Uebou, T. Kiyabul, S. Okada, J. Yamaki, *reports Inst. Adv. Mater. Study Kyushu Univ.* **2002**, *16*, 1.
- [41] F. Lalère, J. B. Leriche, M. Courty, S. Boulineau, V. Viallet, C. Masquelier, V. Seznec, *J. Power Sources* **2014**, *247*, 975.
- [42] Y. Noguchi, E. Kobayashi, L. S. Plashnitsa, S. Okada, J. I. Yamaki, *Electrochim. Acta* **2013**, *101*, 59.
- [43] Z. Deng, G. Sai Gautam, S. K. Kolli, J.-N. Chotard, A. K. Cheetham, C. Masquelier, P. Canepa, *Chem. Mater.* **2020**, *32*, 7908.
- [44] J. Kang, S. Baek, V. Mathew, J. Gim, J. Song, H. Park, E. Chae, A. K. Rai, J. Kim, *J. Mater. Chem.* **2012**, *22*, 20857.
- [45] S. Chen, C. Wu, L. Shen, C. Zhu, Y. Huang, K. Xi, J. Maier, Y. Yu, *Adv. Mater.* **2017**, *29*, DOI 10.1002/adma.201700431.
- [46] M. J. Aragón, P. Lavela, G. F. Ortiz, R. Alcántara, J. L. Tirado, *Inorg. Chem.* **2017**, *56*, 11845.
- [47] Y. Liu, Y. Zhou, J. Zhang, Y. Xia, T. Chen, S. Zhang, *ACS Sustain. Chem. Eng.* **2017**, *5*, 1306.
- [48] R. Rajagopalan, B. Chen, Z. Zhang, X.-L. Wu, Y. Du, Y. Huang, B. Li, Y. Zong, J. Wang, G.-H. Nam, M. Sindoro, S. X. Dou, H. K. Liu, H. Zhang, *Adv. Mater.* **2017**, *29*, 1605694.
- [49] K. Kawai, W. Zhao, S. Nishimura, A. Yamada, *ACS Appl. Energy Mater.* **2018**, *1*, 928.
- [50] R. Liu, G. Xu, Q. Li, S. Zheng, G. Zheng, Z. Gong, Y. Li, E. Kruskop, R. Fu, Z. Chen, K. Amine, Y. Yang, *ACS Appl. Mater. Interfaces* **2017**, *9*, 43632.
- [51] D. Wang, X. Bie, Q. Fu, D. Dixon, N. Bramnik, Y. S. Hu, F. Fauth, Y. Wei, H. Ehrenberg, G. Chen, F. Du, *Nat. Commun.* **2017**, *8*, 1.
- [52] F. Lalère, V. Seznec, M. Courty, J. N. Chotard, C. Masquelier, *J. Mater. Chem. A* **2018**, *6*, 6654.
- [53] T. Zhu, P. Hu, X. Wang, Z. Liu, W. Luo, K. A. Owusu, W. Cao, C. Shi, J. Li, L.

- Zhou, L. Mai, *Adv. Energy Mater.* **2019**, *9*, 2.
- [54] H. Gao, Y. Li, K. Park, J. B. Goodenough, *Chem. Mater.* **2016**, *28*, 6553.
- [55] S. Patoux, G. Rousse, J. B. Leriche, C. Masquelier, *Chem. Mater.* **2003**, *15*, 2084.
- [56] M. V. Zakharkin, O. A. Drozhzhin, I. V. Tereshchenko, D. Chernyshov, A. M. Abakumov, E. V. Antipov, K. J. Stevenson, *ACS Appl. Energy Mater.* **2018**, *1*, 5842.
- [57] H. Li, T. Jin, X. Chen, Y. Lai, Z. Zhang, W. Bao, L. Jiao, *Adv. Energy Mater.* **2018**, *8*, 1801418.
- [58] J. N. Chotard, G. Rousse, R. David, O. Mentré, M. Courty, C. Masquelier, *Chem. Mater.* **2015**, *27*, 5982.
- [59] H. Kabbour, D. Coillot, M. Colmont, C. Masquelier, O. Mentré, *J. Am. Chem. Soc.* **2011**, *133*, 11900.
- [60] F. Hatert, *Acta Crystallogr. Sect. E Struct. Reports Online* **2009**, *65*, i30.
- [61] F. Lalère, V. Seznec, M. Courty, R. David, J. N. Chotard, C. Masquelier, *J. Mater. Chem. A* **2015**, *3*, 16198.
- [62] Z. Jian, C. Yuan, W. Han, X. Lu, L. Gu, X. Xi, Y. S. Hu, H. Li, W. Chen, D. Chen, Y. Ikuhara, L. Chen, *Adv. Funct. Mater.* **2014**, *24*, 4265.
- [63] D. Gryaznov, S. K. Stauffer, E. A. Kotomin, L. Vilčiauskas, *Phys. Chem. Chem. Phys.* **2020**, *22*, 11861.
- [64] M. K. Y. Chan, G. Ceder, *Phys. Rev. Lett.* **2010**, *105*, 196403.
- [65] J. Zhang, G. Liang, C. Wang, C. Lin, J. Chen, Z. Zhang, X. S. Zhao, *ACS Appl. Mater. Interfaces* **2020**, DOI 10.1021/acsami.0c07702.
- [66] O. Tillement, J. C. Couturier, J. Angenault, M. Quarton, *Solid State Ionics* **1991**, *48*, 249.
- [67] G. Bergerhoff, R. Hundt, R. Sievers, I. D. Brown, *J. Chem. Inf. Comput. Sci.* **1983**, *23*, 66.
- [68] M. V. Zakharkin, O. A. Drozhzhin, S. V. Ryazantsev, D. Chernyshov, M. A. Kirsanova, I. V. Mikheev, E. M. Pazhetnov, E. V. Antipov, K. J. Stevenson, *J. Power Sources* **2020**, *470*, 228231.
- [69] "Basic inorganic chemistry - CERN Document Server," **n.d.**
- [70] J. Gopalakrishnan, K. K. Rangan, *Chem. Mater.* **1992**, *4*, 745.
- [71] A. Jain, S. P. Ong, G. Hautier, W. Chen, W. D. Richards, S. Dacek, S. Cholia, D. Gunter, D. Skinner, G. Ceder, K. A. Persson, *APL Mater.* **2013**, *1*, 011002.
- [72] H. Wang, C. Chen, C. Qian, C. Liang, Z. Lin, *RSC Adv.* **2017**, *7*, 33273.
- [73] B. Manoun, A. El Jazouli, S. Krimi, A. Lachgar, *Powder Diffr.* **2004**, *19*, 162.
- [74] G. Kresse, J. Furthmüller, *Phys. Rev. B - Condens. Matter Mater. Phys.* **1996**, *54*, 11169.
- [75] G. Kresse, J. Furthmüller, *Comput. Mater. Sci.* **1996**, *6*, 15.
- [76] J. P. Perdew, K. Burke, M. Ernzerhof, *Phys. Rev. Lett.* **1996**, *77*, 3865.
- [77] M. Cococcioni, S. De Gironcoli, *Phys. Rev. B - Condens. Matter Mater. Phys.* **2005**, *71*, 035105.
- [78] S. Dudarev, G. Botton, *Phys. Rev. B - Condens. Matter Mater. Phys.* **1998**, *57*, 1505.
- [79] A. Jain, G. Hautier, C. J. Moore, S. Ping Ong, C. C. Fischer, T. Mueller, K. A. Persson, G. Ceder, *Comput. Mater. Sci.* **2011**, *50*, 2295.
- [80] L. Wang, T. Maxisch, G. Ceder, *Phys. Rev. B - Condens. Matter Mater. Phys.* **2006**, *73*, 195107.

- [81] J. D. Pack, H. J. Monkhorst, *Phys. Rev. B* **1977**, *16*, 1748.
- [82] S. P. Ong, W. D. Richards, A. Jain, G. Hautier, M. Kocher, S. Cholia, D. Gunter, V. L. Chevrier, K. A. Persson, G. Ceder, *Comput. Mater. Sci.* **2013**, *68*, 314.
- [83] P. P. Ewald, *Ann. Phys.* **1921**, *369*, 253.